




Synthesis and characterization of InP quantum dots for photovoltaics applications

Dina Lasheen¹, Marwa Fathy^{2,*} , Hossam Awad Othman¹, Meawad Mohamed Elkholy^{1,3}, and Abd El Hady B. Kashyout²

¹ Physics Department, Faculty of Science, Menoufia University, Shibin al-Kawm, Egypt

² Electronic Materials Department, Advanced Technology and New Materials Institute, City of Scientific Research and Technological Applications, New Borg Al-Arab, Alexandria, Egypt

³ Physics Department, Faculty of Science, New Mansoura University, New Mansoura, Dakahlia, Egypt

Received: 20 November 2022

Accepted: 26 February 2023

Published online:
29 March 2023

© The Author(s) 2023

ABSTRACT

In this article, InP quantum dots (QDs) are synthesized with a green methodology. The preparation of the InP QDs is demonstrated by varying the ratios of the precursors used such as InCl₃ and trioctylphosphine (TOP). These QDs are fabricated through the application of TOP (as phosphorous source and reducing agent for the In salt) for forming indium and to develop the targeted InP QDs, which are characterized using HRTEM, XRD, PL, FTIR, UV-Vis, and time resolved spectroscopy. A rapid reaction time (~ 30 min) procedure in a single pot at a temperature of ~ 310 °C is developed. InP QDs with particle sizes varying from 4 to 6 nm have been measured with different concentrations of InCl₃ and TOP. InP QDs yield reached 23%. Zincblende crystal structure is recognized for InP with high orientation plane of (220) as confirmed with XRD and confirmed with SAED. Solar cell devices are built by anchoring the InP QDs onto a TiO₂ layer and measure the photovoltaic performance and spectral response of the device built on FTO/glass substrate. TiO₂/InP QDs solar cell devices are fabricated with high fill factor of 0.86 and open circuit voltage value of 501 mV and overall efficiency of 0.48%.

1 Introduction

Semiconductor quantum dot nanomaterials (QDs) have unique nanocrystalline structure (nano-sized) which boost their electrical and optical properties [1, 2]. The size of the nanoparticles is in the range of QDs that can be 2–10 nm [3]. Generally, there are many groups such as II–VI, III–V, and IV–VI to

compose wide varieties of QD compounds. Quantum confinement is the key to produce nanomaterials with this unique size which makes them have a tunable bandgap [4]. The quantum confinement is a special one of the electron–hole pairs (excitons) in one or more dimensions through some types of materials. 3D confinement (QD), 2D confinement as (quantum wire), and 1D confinement (quantum well) have

Address correspondence to E-mail: mbahnase@srtacity.sci.eg

attracted many researchers around the world for their great variety of applications [5]. QDs are synthesized by physical [5, 6], chemical [7], and biogenic approaches [8]. Chemical approaches are used in QDs fabrication and applied in many optoelectronic devices [9]. Many synthesis procedures are used to provide QDs such as colloidal methods [10] and epitaxial growth [11].

InP QDs have attracted a great interest due to being environmentally friendly in the applications of light emitting diodes, used as fluorescent probes in biological labeling, QD solar cells and other fields [12]. In general, the prepared InP QDs have low luminescence value due to the existence of non-radiative channels originating from surface states [13]. But, it is a promising compound due to its tunable band gap from bulk material (1.35 eV at 300 K) to be a wide band gap with values varying from 1.5 to 3.5 eV for the QDs structure [14]. Colloidal InP QDs are known to be of high quality that having semiconductor behavior due to their low ionic lattice value, higher value of Bohr radii and less toxic when compared to other QDs such as CdS, CdTe, and CdSe. Consequently, they have attracted great interest in many applications such as photovoltaic solar cells, light emitting diodes, and other photoelectric devices [15]. InP QDs are difficult to be fabricated through the conventional chemical methods that have failed to match with the needed high quality of the QDs such as narrow size distribution and crystallinity [16, 17]. Indium precursors choices have many varieties, but phosphorus precursors are not familiar [15]. The most known phosphorous precursor is Tris(trimethylsilyl)phosphine [P(SiMe₃)₃]. However, it is known to be with high toxicity, flammable, high-priced, and banned in Europe [15].

New synthesis methods utilized alternate sources of phosphorous. They used phosphine gas (PH₃) as the source of phosphorous but it is considered also as high toxic and scarce [8]. So, an alternative source of safe phosphorous should be explored.

Recently, trioctylphosphine (TOP) is considered as a promising precursor [18]. It is used to fabricate many metal phosphides such as Rh₂P [19], PdP₂ [20], Ni₂P [21], and InP [15]. InP nanoparticles were synthesized using TOP with many impurities that have been found and large size nanoparticles from 15 nm to micron size [22]. Recently, prepared InP QDs from InCl₃ and TOP have been obtained with 2.05 nm [15].

In this work, various concentrations of TOP and InCl₃ are used to synthesize InP QDs in octadecene as non-coordinating solvent and optimizing the preparation conditions of this green methodology. This method introduced a rapid reaction time (~ 30 min) procedure in a single pot at a temperature of ~ 310 °C. The produced QDs with Zincblende crystal structure have small size distribution, which is greatly affect the efficiency and quantum yield of its photoluminescence (PL) efficiency because it depends on the surface to volume ratio of the QDs. Also, TiO₂/InP solar cell devices are fabricated and evaluated.

2 Experimental work

InP QDs are synthesized through a methodology of applying a one pot procedure through the hot injection technique that is applied to the growth of the QDs at high temperature (~ 310 °C).

2.1 InP QDs synthesis

For InP QDs synthesis: four samples of InP QDs are prepared with varying the ratios of indium chloride to TOP as shown in Table 1. Figure 1 shows the steps of InP QDs fabrication procedure with all experimental parameters. In a three neck round flask, a certain weight (wt%) of indium chloride and octadecene are mixed together in the round flask under an argon atmosphere (gas purity of 99%) as indicated in Table 1. The mixture is heated up to 310 °C and TOP is rapidly injected into the flask. The produced InP QDs are grown at a temperature of ~ 270 °C for a time interval of < 5 min. The resulted QDs are cooled down to room temperature under argon gas atmosphere.

For QDs cleaning, the synthesized InP QDs are washed in a mixture of methanol and *n*-hexane with a ratio of 1:1 at RT. This mixture is heated to a temperature of 60 °C and few drops of acetone are added. The cleaning process is done several times to remove the excess of the existed organic ligands. After cleaning, the solution is centrifuged for 20 min. at 6000 rpm with *n*-hexane to remove the unreacted TOP, then the nanopowder of InP QDs is separated and dried at a temperature of 70 °C for 2 h and a yield of 23% is achieved for the net InP QDs.

Table 1 InP QDs preparation parameters, calculated crystallite size and determined band gap from UV–Vis and PL data

Sample	InCl ₃ (g)	Octadecene (ODE)	TOP (tri- <i>n</i> -octyl phosphine) (ml)	Crystallite size, <i>D</i> (nm)	Injection temperature (°C)	Band gap (<i>E_g</i>) (eV)	
						UV–Vis	PL
S1	0.48	6 ml	4	2.39	310	2.08	2.33, 2.54
S2	0.16		4	2.9		2.51	2.32, 2.51
S3	0.16		6	2.92		2.4	2.31, 2.53
S4	0.16		8	2.37		2.1	2.33, 2.54

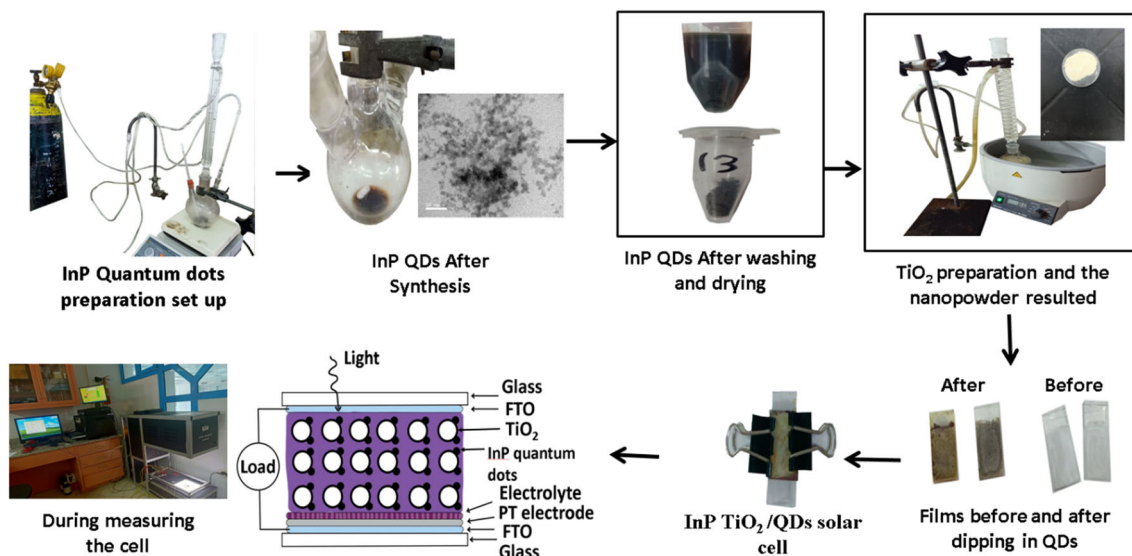


Fig. 1 Experimental set-up for the hot injection InP synthesis and the resulted nano powder and their TiO₂/InP solar cell device

2.2 Manufacturing of InP QDs embedded in TiO₂ for solar cells applications

TiO₂/InP QDs solar cell device is fabricated as follows: a substrate of FTO/glass has a measured sheet resistance value of 7 Ω/sq is cleaned with distilled water then in acetone and using an ultrasonic bath for 20 min. to remove any undesired substances on its surface. TiO₂ nanopowder is prepared according to Kashyout et al. [9, 23] with particle size in range between 20 and 30 nm. A thin layer of TiO₂ paste is applied on the FTO glass by using the doctor blade technique and heat treated to form successive 3–4 thin layers at 450 °C for 30 min. A total thickness of TiO₂ reached ~ 14 μm [24–26].

TiO₂ films are dipped in the InP colloidal solution which is dissolved in toluene and left for 24 h until its color changed from white to black (Fig. 1), then washed by toluene to be used in the solar cell devices measurement [27].

Pt counter electrode is prepared on FTO/glass substrates using DC sputtering technique [28]. It is applied directly on the top of QDs/TiO₂ working electrode. Both electrodes are clamped tightly together as shown in Fig. 1. To connect the working and the counter electrodes, an electrolyte has the chemical formula of 0.5 M LiI/50 mM I₂ in (3-methoxypropionitrile) is dropped between the two electrodes.

2.3 Characterizations

The structure of the InP QDs are confirmed by X-ray diffractometer (XRD) (Shimadzu 7000, Japan), Fourier transform infrared spectroscopy (FT-IR) spectra (Shimadzu FTIR-8400 S, Japan). Morphology and particle size of the InP QDs are observed and measured by high-resolution transmission electron microscopy (HRTEM; JEOL-JEM-2100, Japan). PL and absorption spectra are analyzed by using double-beam UV-Vis spectrophotometer (LABOMED) with spectrum ranging from 190 to 1100 nm. In order to determine the life time of emission of InP QDs is measured using the imaging microscope (FLIM system Alba with v5 from ISS) for determining the electron lifetime. For the excitation process, a laser diode of is excite at a wavelength of 640 nm, which is coupled with scanning module of (ISS) through multi-band dichroic filter to epifluorescence microscope (Model IX73, Olympus, Tokyo, Japan).

The external quantum efficiency (EQE) of the fabricated InP QDs solar cell is *determined* using a monochromator utilizing a PVE300 system in a Bentham TMc300 with a 300 nm focal length monochromator.

The solar cell performance of the TiO₂/InP QDs is measured using PET Photo Emission Tech, Inc., USA as solar simulator device. The efficiency (η) can be calculated from Eq. 1 [8].

$$\eta \% = (J_{sc} V_{oc} FF / I_0) \times 100\%, \quad (1)$$

where J_{sc} is the short circuit current density (mA/cm²), V_{oc} is the open circuit voltage (V), and FF is the fill factor.

3 Results and discussion

3.1 Structural analysis

3.1.1 XRD analysis

The XRD patterns of InP synthesized QDs for the four samples as illustrated in Table 1 to produce indium phosphide QDs are shown in Fig. 1. According to JCPDS card of InP QDs, the main peaks are detected at 2θ of (21°, 32°, 43.6°, 54.1°, 56.1°, and 63.8°). These peaks' positions match with InP Zincblende structure (JCPDS Card No. 03-065-2889) for the planes (111), (200), (220), (311), (222), and (400), respectively. Also,

XRD of Indium metal (JCPDS Card No. 03-065-9682) [26] is detected in samples S1 and S4 with lower intensities than the InP structure. The inserted table in Fig. 2 shows the 2θ values with their corresponding planes for both InP and In structures. By applying Scherrer's equation, the InP QDs crystallite size is calculated as follows [29]:

$$D = \frac{k\lambda}{\beta \cos\theta}. \quad (2)$$

The average crystallite size is D , the X-ray wavelength is λ , the width of the X-ray peak on the 2θ axis is β , which is defined from the full width at half maximum (FWHM), the Bragg angle is θ , and K is the Scherrer's constant. K depends on the crystallite shape and the size distribution, indices of the diffraction line, and the actual definition used for β whether FWHM or integral breadth [30, 31]. In this work, $K = 0.9$ is used. Further, microstrain in the crystallites or nanocrystals also affects the width β , which needs to be considered in an accurate analysis. Spatial fluctuations in the alloy composition can also affect the width. In this work, the calculated values of D values ranged from 2.37 nm (S4) to 2.39 nm (S1), 2.9 nm (S3), and 2.92 nm (S2) as shown in Table 1.

3.1.2 FTIR analysis

FTIR spectra of the produced compounds are shown in Fig. 3. Number of characteristic peaks are observed at 2854 cm⁻¹, 2915 cm⁻¹, 801 cm⁻¹, and 715 cm⁻¹, corresponding to C-H stretching modes for the CH₂ and CH₃ groups, which may be originated from the alkane molecules from TOP adsorbed on the surface of the InP QDs [32]. Peaks at 1456–1452 cm⁻¹ correspond to the vibrational frequencies of -CH₂Cl or for -CH₃ [29]. Other peaks at 801–715 cm⁻¹ may be attributed to C-Cl conformational sensitive stretch modes of chlorooctane (C₈H₁₇Cl) [32], which resulted from the reaction of chlorine ions with C₈H₁₇ ion (resulted from P-C cleavage of TOP). The strong bands appeared at 1054–1128 cm⁻¹ associated with InP capped with TOP [22]. A peak at 1620 cm⁻¹ that appeared in the spectra of S2 and S3 is corresponded to C-C in chlorooctane which assure the reaction mechanism as shown in Eqs. 3–7.



Fig. 2 XRD patterns of the prepared InP QDs samples (according to JCPDS of InP: 03-065-2889 and JCDPS of In metal: 03-065-9682)

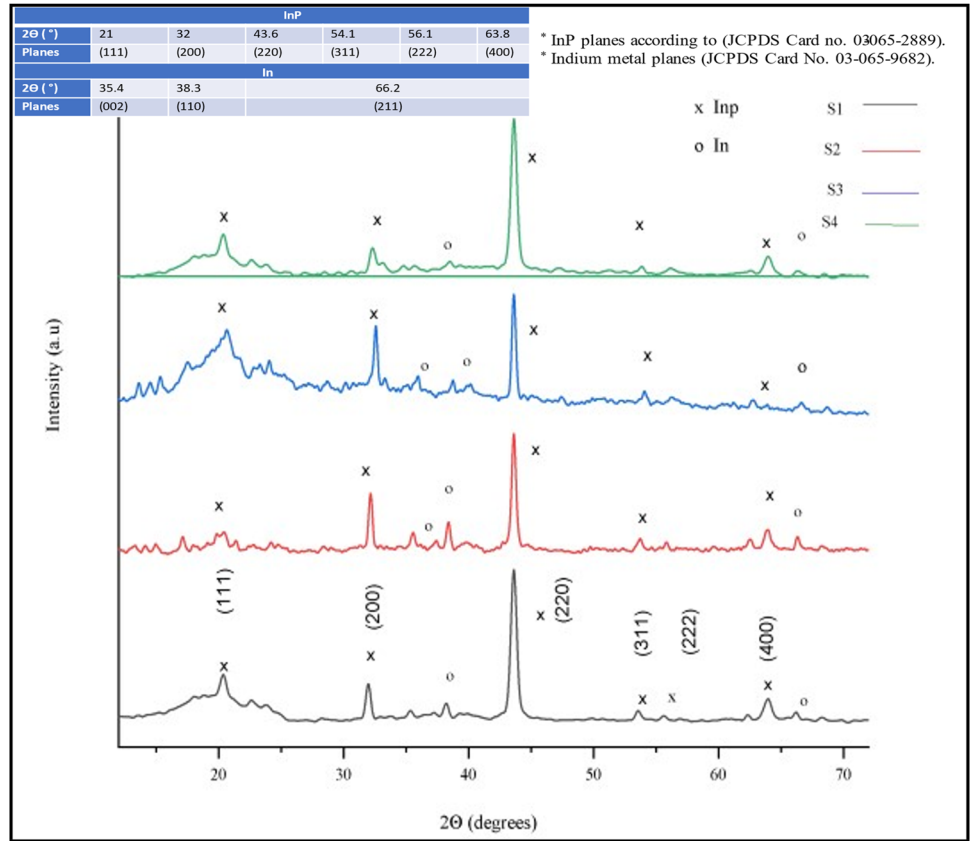
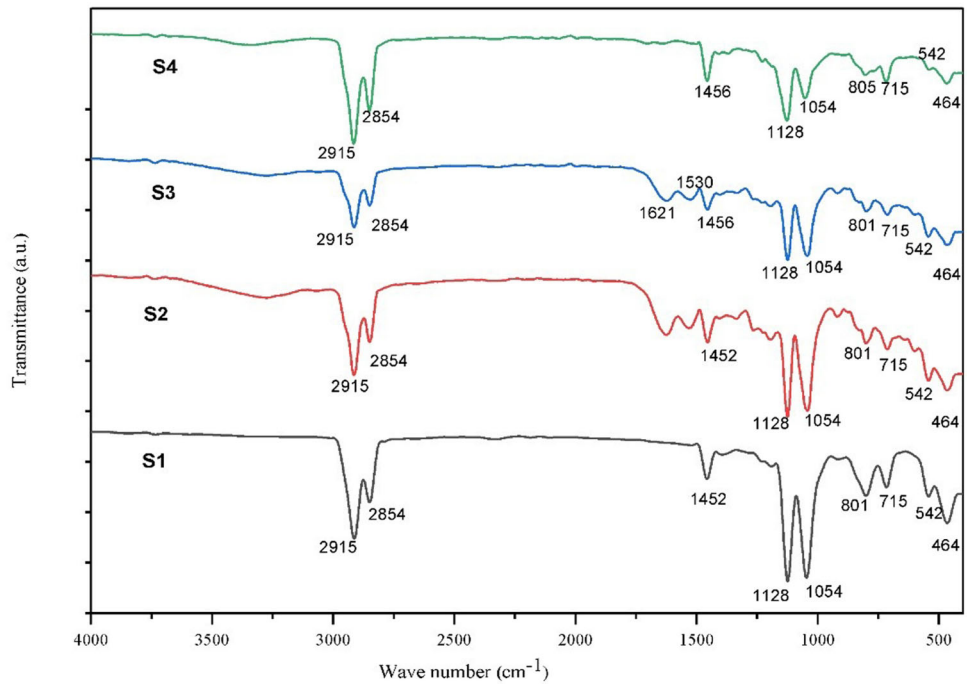
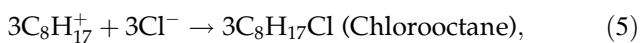
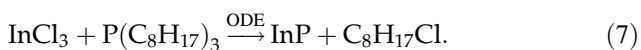


Fig. 3 FTIR spectra of the prepared InP QDs using different TOP concentrations





Overall Reaction:



3.1.3 HRTEM analysis

Figure 4 shows HRTEM images of sample S3 in Table 1. They clearly indicate well crystallized homogeneous QD nanoparticles with an average particle size ranging from 4 to 6 nm (Fig. 4a, b, e), which is comparable with the calculated crystallite size for the same sample of 2.9 nm as shown in Table 1. Selected area electron diffraction (SAED) in Fig. 4c shows the polycrystalline nature of the InP

QDs with the (111), (200), (222), and (400) planes, with a *d* spacing value of 3.1 Å as shown in Fig. 4d.

3.2 Optical analysis

PL refers to the peaks obtained when the samples are excited at a certain wavelength [32]. For the prepared InP QDs, the excitation process is occurred using laser beam with an excitation mode at a wavelength of 365 nm. Figure 5 displays the PL spectra of InP samples, where they exhibit the impact of quantum confinement in the absorption spectra. With an onset that corresponds to the particle size, these particles absorb light in the visible spectrum. As shown in Fig. 5, each sample have two peaks one at λ of 475 nm ($E_g = 2.61$ eV) and another at λ of 530 nm ($E_g = 2.34$ eV). This means that the QDs have two different particle sizes as confirmed and observed from HRTEM measurement.

Figure 6a shows the UV–Vis absorbance spectra of InP QDs samples which dissolved in toluene

Fig. 4 HRTEM micrographs of the prepared InP QDs (a, b, e), SAED (c), and *d*-spacing (e)

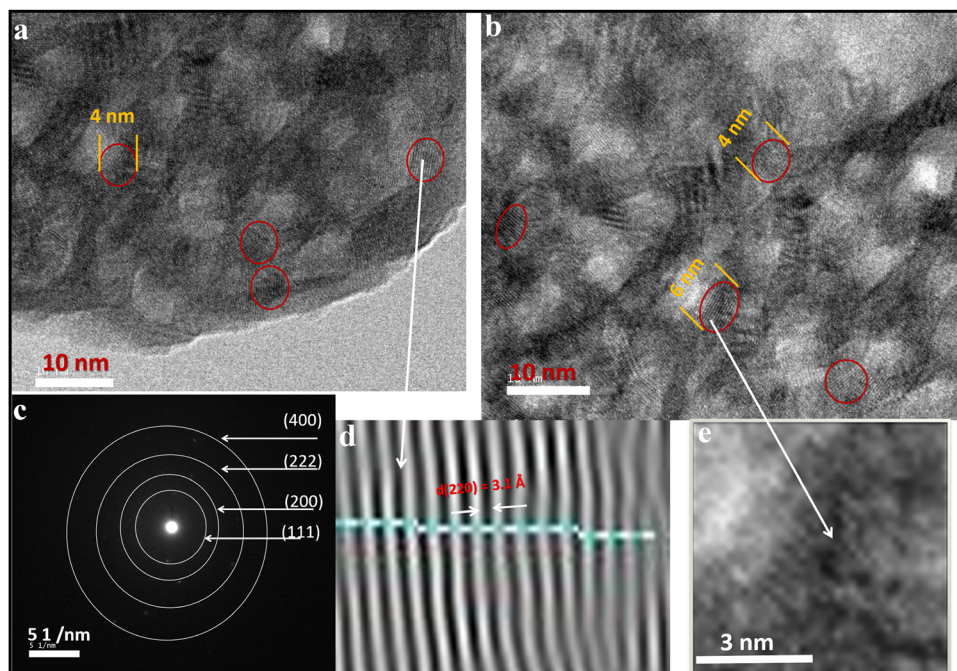
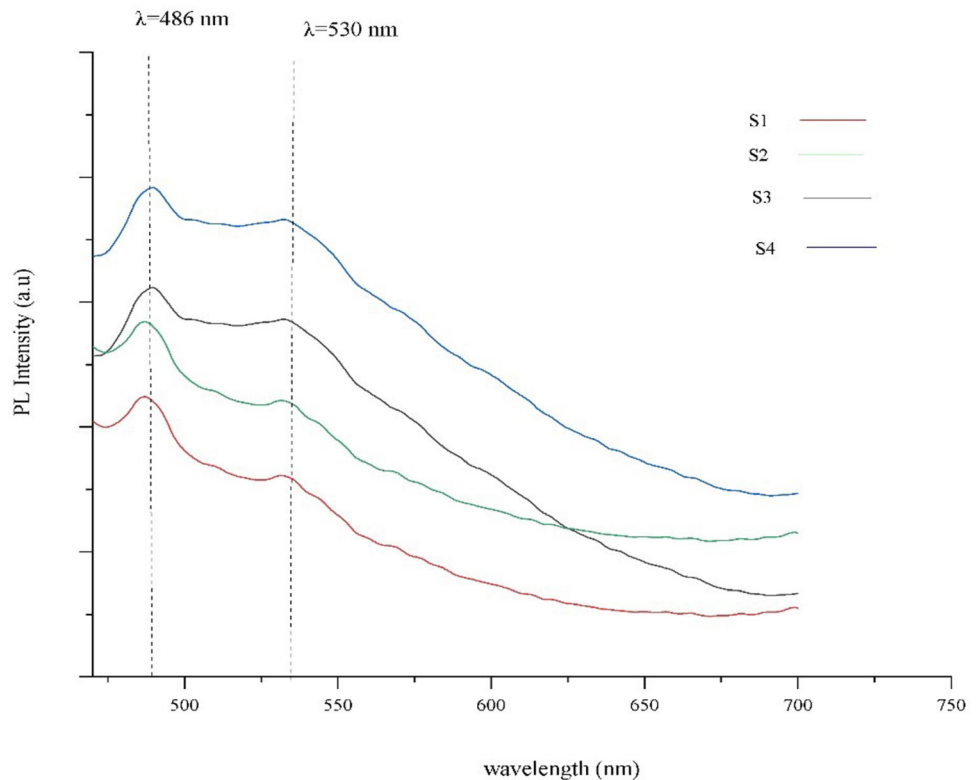


Fig. 5 PL spectra of prepared InP QDs with different TOP concentrations



solution. It shows the peaks which are centered at about 590 nm. The calculated band gap using the UV–Vis spectrum of S3 has been calculated from the straight line that cut the X-axis and gives a band gap of 2.4 eV as shown in Fig. 6c, which matches with the results from PL measurements. The InP QDs has a direct band gap transition and this means that the crystal momentum of electrons and holes is the same in both the conduction and valence bands [13].

The optical transmittance of sample S3 is measured and shown in Fig. 6c which shows a low value of about 10%.

Figure 7a, b shows the fluorescence lifetime imaging (FLIM) which presents the differences in the excited state decay rate from the InP sample (S3) and it shows the raw FLIM data with PL intensity decay. This decay curve is fitted by the sum of exponential functions and having 1.9 ns lifetime [33].

Figure 8 shows the measurement of the relative quantum efficiency of the fabricated InP solar cell at room temperature (sample 3). The peak is observed at the region of 700 to 800 nm with a value of relative quantum efficiency of about 3.34% compared with the previous published work which indicate the high sensitivity of the produced InP to the incident

photons. But, the appearance of the EQE peak at high value of wavelength indicate the carrier generation is not very high and the recombination of the generated carriers on the surface of TiO_2 surface may be occurred [29, 34].

3.2.1 I–V curve of TiO_2/InP QDs solar cell

For the fabricated solar cell using sample S3 of InP, the efficiency (η) is measured by using solar simulator instrument as shown in Fig. 9. The solar cell output values of TiO_2/InP QDs solar cell device are J_{sc} of 1.04 mA/cm^2 , V_{oc} of 501 mV, FF of 86.4, and cell efficiency of 0.48%. From the literature, the best TiO_2/InP QDs solar cell which using the same cell component has J_{sc} of about 8.3 mA/cm^2 , V_{oc} about 237 mV, FF of 33, and efficiency of 0.64% [35]. By comparing these data with the literature, the preparation technique that is used is a promising method. We get a good open circuit voltage and fill factor. But, the short circuit current density is not high. It may be attributed to the low value of InP QDs life time and this value can be modified by increasing the purity of the InP QDs by more washing which will enhance the efficiency. The high fill factor of the cell means that it is stable and the good open circuit voltage of the cell

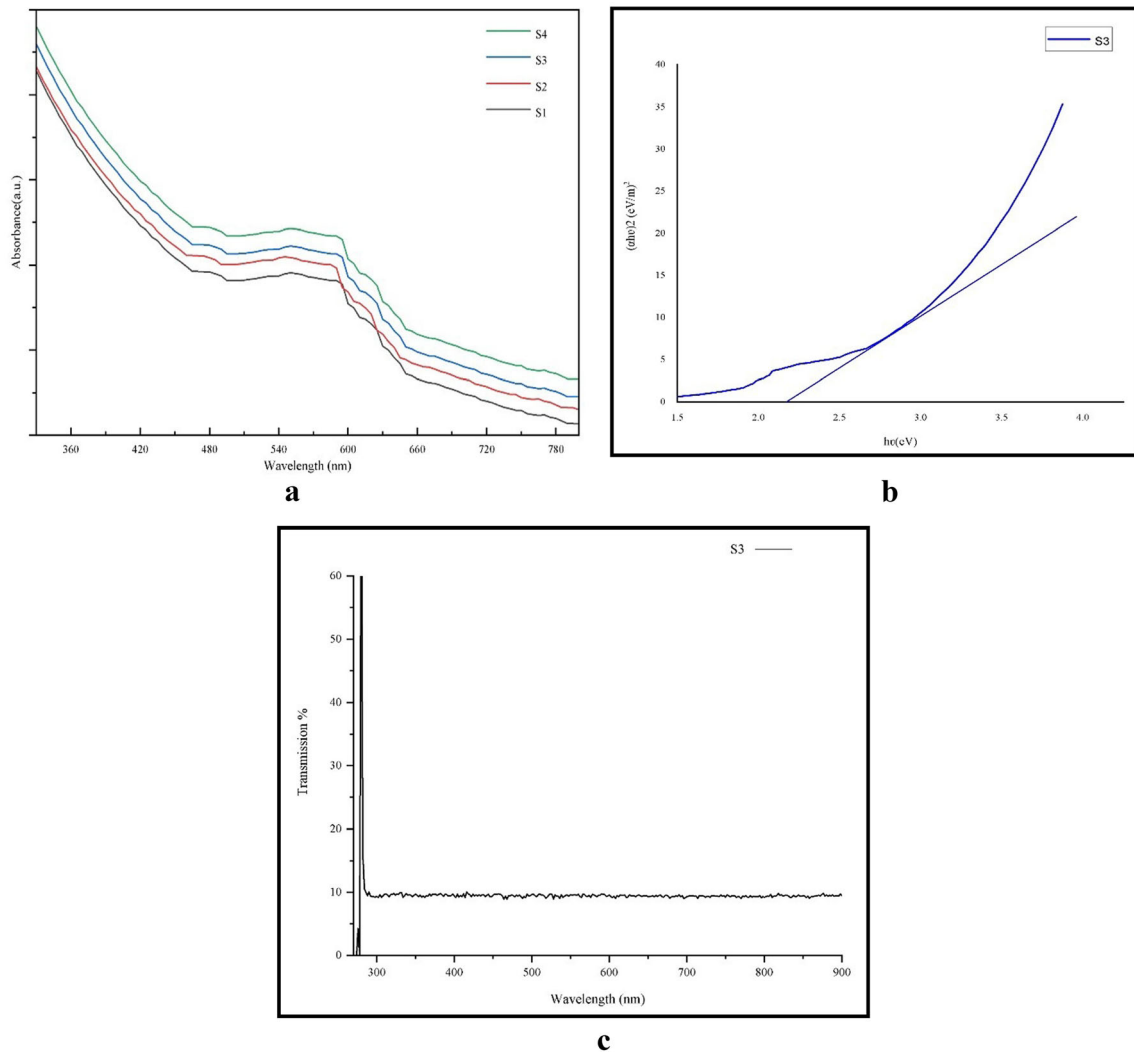


Fig. 6 **a** UV–Vis absorption spectra of all samples, **b** calculated band gap energy of InP QDs (S3) and **c** transmission spectrum of sample S3

Fig. 7 **a** Fluorescence lifetime imaging (FLIM) and **b** the measured and fitted decay time for sample 3

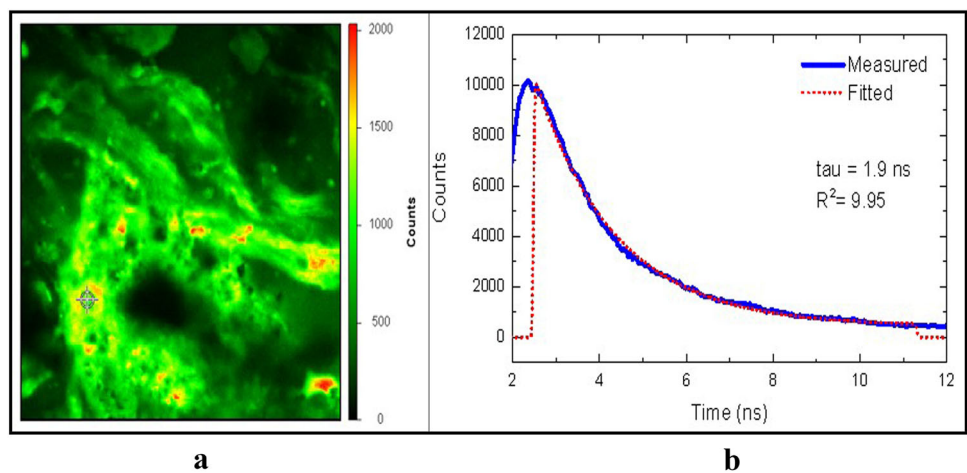


Fig. 8 Quantum efficiency measurements for InP (S3)/TiO₂ QDs solar cell

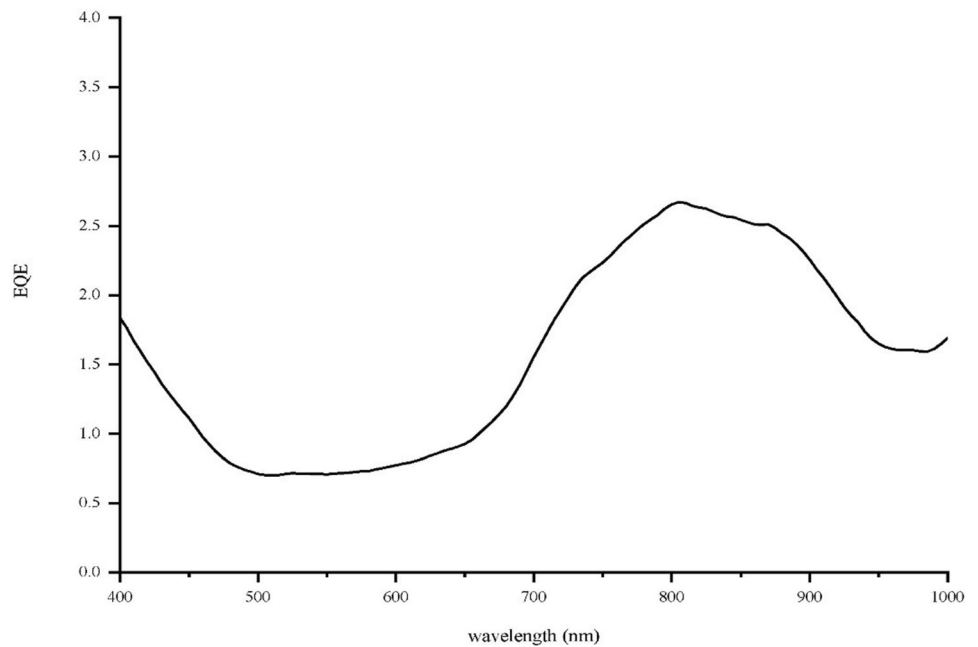
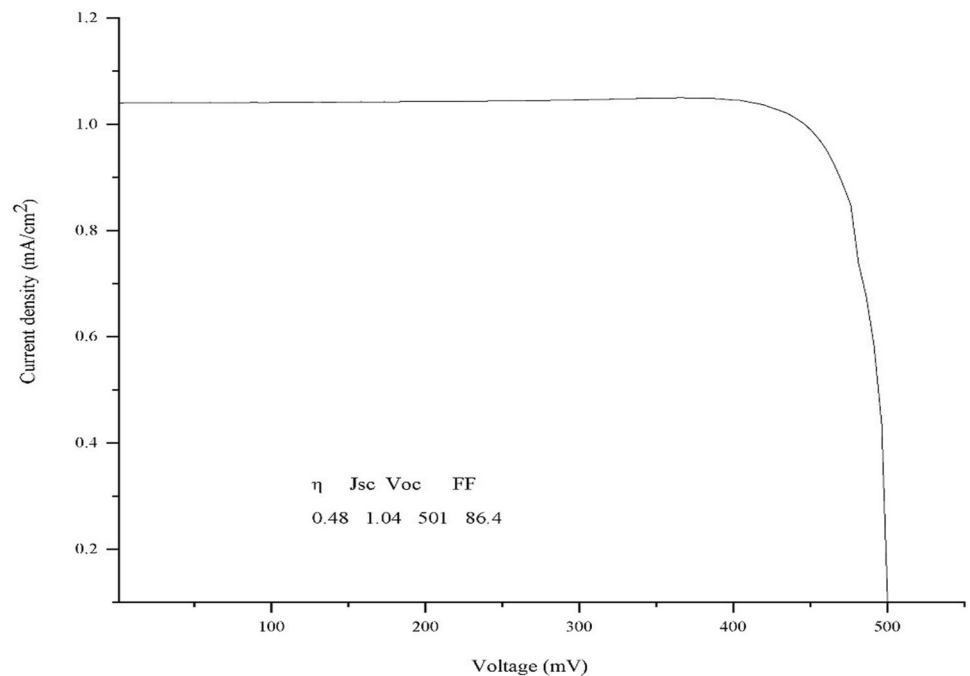


Fig. 9 Current density–voltage (*J–V*) curve of the prepared InP/TiO₂ QDs solar cell



means good connection in the cell. The low value of the short circuit current density may be attributed to number of reasons such as capping ligand is not applied in the synthesis procedure, which may improve the adsorption of the QDs on the surface of TiO₂ particles as well as we applied iodide/triiodide electrolyte which generated lower values of photocurrent [36].

4 Conclusion

Successful synthesis of InP QDs with a green and fast way by using hot injection technique and non-toxic precursors of TOP. InP QDs are used for QDSC applications. High quality narrow range InP QDs of particle size varying from 4 to 6 nm is synthesized. Zincblende crystal structure with high orientation of

(220) plane is detected, which is also confirmed from SAED measurements. A high yield InP QDs reaching 23% and good InP QDs/TiO₂ solar cell device is built up (as the working electrode) and measured to yield high fill factor (0.86) and open circuit voltage (501 mV) and efficiency of 0.48%. Lower values of short circuit current density is attained, which need further work on more QDs purification, capping ligand application and changing the ion electrolytes for higher charge mobility. EQE of 3.34% is measured in the visible range with a life time of 1.9 ns for the electrons in the fabricated InP QDs.

Acknowledgements

The authors wish to express their thanks to the Department of Electronic Materials, Institute of Advanced Technology and New Materials, SRTA City, Egypt, and Physics Department, Faculty of Science, Menoufia University, Shebin Elkom, Egypt. Special thanks to Professor Badawi Anis, National Research Centre (NRC), Egypt and Professor Ahmed Mortada, Central of Metallurgical Research and Development institute (CMRDI), Egypt.

Author contributions

Conceptualization, AEHBK, HAO, MME, MF and DL; Material preparation, AEHBK, MF and DL; Validation, AEHBK, HAO, MME, MF and DL; Data collection, AEHBK, MF and DL; Analysis, AEHBK, MF and DL; Resources, AEHBK, MF and DL; Data curation, AEHBK, MF and DL; Writing—the first draft, AEHBK, MF and DL; Writing—review and editing, AEHBK, MF, HAO, MME and DL; Supervision, AEHBK, HAO, MME and MF. All authors commented on previous versions of the manuscript. All authors read and approved the final manuscript.

Funding

Open access funding provided by The Science, Technology & Innovation Funding Authority (STDF) in cooperation with The Egyptian Knowledge Bank (EKB). The authors declare that no fund, grants, or other support were received during the preparation of this manuscript.

Data availability

All data generated or analyzed during this study are included in this published article.

Declarations

Conflict of interest The authors declare no conflict of interest. The authors have no relevant financial or non-financial interests to disclose.

Open Access This article is licensed under a Creative Commons Attribution 4.0 International License, which permits use, sharing, adaptation, distribution and reproduction in any medium or format, as long as you give appropriate credit to the original author(s) and the source, provide a link to the Creative Commons licence, and indicate if changes were made. The images or other third party material in this article are included in the article's Creative Commons licence, unless indicated otherwise in a credit line to the material. If material is not included in the article's Creative Commons licence and your intended use is not permitted by statutory regulation or exceeds the permitted use, you will need to obtain permission directly from the copyright holder. To view a copy of this licence, visit <http://creativecommons.org/licenses/by/4.0/>.

References

1. G.L. Yang, H.Z. Zhong, Organometal halide perovskite quantum dots: synthesis, optical properties, and display applications. *Chin. Chem. Lett.* (2016). <https://doi.org/10.1016/j.ccl.2016.06.047>
2. H. Seo, J.H. Park, O.H. Kwon, O.P. Kwon, S.K. Kwak, S.W. Kim, Highly qualified InP based QDs through a temperature controlled ZnSe shell coating process and their DFT calculations. *Nanoscale Adv.* (2020). <https://doi.org/10.1039/D0NA00451K>
3. L. Pitkänen, A.M. Striegel, Size-exclusion chromatography of metal nanoparticles and quantum dots. *Trends Anal. Chem.* (2016). <https://doi.org/10.1016/j.trac.2015.06.013>
4. A.B. Kashyout, H. Soliman, M. Fathy, E.A. Gomaa, A.A. Zidan, CdSe quantum dots for solar cell devices. *Int. J. Photoenergy* (2012). <https://doi.org/10.1155/2012/952610>
5. G. Ramalingam, P. Kathirgamanathan, G. Ravi, T. Elangovan, B. Arjunker, N. Manivannan, K. Kasinathan, *Quantum Confinement* (IntechOpen, 2020). <https://doi.org/10.5772/intechopen.90140>

6. M.A. Reed, Quantum dots. *Sci. Am.* (1993). <https://doi.org/10.1038/scientificamerican0193-118>
7. A.E.H.B. Kashyout, M. Fathy, M.B. Soliman, Studying the properties of RF-sputtered nanocrystalline tin-doped indium oxide. *Int. J. Photoenergy* (2011). <https://doi.org/10.1155/2011/139374>
8. L. Li, M. Protière, P. Reiss, Economic synthesis of high quality InP nanocrystals using calcium phosphide as the phosphorus precursor. *Chem. Mater.* (2008). <https://doi.org/10.1021/cm7035579>
9. A.B. Kashyout, M. Soliman, M. Fathy, Effect of preparation parameters on the properties of TiO₂ nanoparticles for dye sensitized solar cells. *Renew. Energy* (2010). <https://doi.org/10.1016/j.renene.2010.04.035>
10. Y. Shirasaki, G.J. Supran, M.G. Bawendi, V. Bulović, Emergence of colloidal quantum-dot light-emitting technologies. *Nat. Photonics* (2013). <https://doi.org/10.1038/nphoton.2012.328>
11. L.N. McCabe, J.M. Zide, Techniques for epitaxial site-selective growth of quantum dots. *J. Vacuum Sci. Technol. A* (2021). <https://doi.org/10.1116/6.0000623>
12. B. Chen, D. Li, F. Wang, InP quantum dots: synthesis and lighting applications. *Small* (2020). <https://doi.org/10.1002/sml.202002454>
13. P.T. Thuy, U.T.D. Thuy, T.T.K. Chi, L.Q. Phuong, N.Q. Liem, L. Li, P. Reiss, Time-resolved photoluminescence measurements of InP/ZnS quantum dots. *J. Phys. Conf. Ser.* (2009). <https://doi.org/10.1088/1742-6596/187/1/012014>
14. E. Jang, Y. Kim, Y.H. Won, H. Jang, S.M. Choi, Environmentally friendly InP-based quantum dots for efficient wide color gamut displays. *ACS Energy Lett.* (2020). <https://doi.org/10.1021/acsenergylett.9b02851>
15. A. Singh, P. Chawla, S. Jain, S.N. Sharma, Tapping the potential of Trioctylphosphine (TOP) in the realization of highly luminescent blue-emitting colloidal indium phosphide (InP) quantum dots. *Phys. E.* (2017). <https://doi.org/10.1016/j.physe.2017.03.029>
16. O.I. Micic, C.J. Curtis, K.M. Jones, J.R. Sprague, A.J. Nozik, Synthesis and characterization of InP quantum dots. *J. Phys. Chem.* (1994). <https://doi.org/10.1021/j100070a004>
17. O.I. Micic, J.R. Sprague, C.J. Curtis, K.M. Jones, J.L. Machol, A.J. Nozik, N.J. Peyghambarian, Synthesis and characterization of InP, GaP, and GaInP₂ quantum dots. *J. Phys. Chem.* (1995). <https://doi.org/10.1021/j100019a063>
18. A.E. Henkes, R.E. Schaak, Trioctylphosphine: a general phosphorus source for the low-temperature conversion of metals into metal phosphides. *Chem. Mater.* (2007). <https://doi.org/10.1021/cm071021w>
19. H. Duan, D. Li, Y. Tang, Y. He, S. Ji, R. Wang, Y. Li, High-performance Rh₂P electrocatalyst for efficient water splitting. *J. Am. Chem. Soc.* (2017). <https://doi.org/10.1021/jacs.7b01376>
20. H. Xie, Q. Geng, X. Zhu, Y. Luo, L. Chang, X. Niu, X. Sun, PdP₂ nanoparticles-reduced graphene oxide for electrocatalytic N₂ conversion to NH₃ under ambient conditions. *J. Mater. Chem.* (2019). <https://doi.org/10.1039/D0TA04709K>
21. P. Nagababu, S.A.M. Ahmed, Y.T. Prabhu, S. Bhowmick, S.S. Rayalu, Synthesis of Ni₂P/CdS and Pt/TiO₂ nanocomposite for photoreduction of CO₂ into methanol. *Sci. Rep.* (2021). <https://doi.org/10.1038/s41598-021-87625-w>
22. P.K. Khanna, K.W. Jun, K.B. Hong, J.O. Baeg, G.K. Mehrotra, Synthesis of indium phosphide nanoparticles via catalytic cleavage of phosphorus carbon bond in *n*-Trioctylphosphine by indium. *Mater. Chem. Phys.* (2005). <https://doi.org/10.1016/j.matchemphys.2004.12.029>
23. M. Fathy, H. Hamad, A.E.H.B. Kashyout, Influence of calcination temperatures on the formation of anatase TiO₂ nano rods with a polyol-mediated solvothermal method. *RSC Adv.* (2016). <https://doi.org/10.1039/C5RA26739K>
24. M. Fathy, H. Hassan, H. Hafez, M. Soliman, F. Abulfotuh, A.E.H.B. Kashyout, Simple and fast microwave-assisted synthesis methods of nanocrystalline TiO₂ and rGO materials for low-cost metal-free DSSC applications. *ACS Omega* (2022). <https://doi.org/10.1021/acsomega.2c01455>
25. M. Fathy, J. El Nady, M. Muhammed, S. Ebrahim, M.B. Soliman, A.B. Kashyout, Quasi-solid-state dye sensitized solar cells based on nanofiber PMA–PVDF and PMA–PVDF/PEG membranes. *Int. J. Electrochem. Sci.* (2016). <https://doi.org/10.1021/acsomega.2c01455>
26. M. Fathy, A.B. Kashyout, J. El Nady, S. Ebrahim, M. Soliman, Electrospun polymethyl acrylate nanofibers membranes for quasi solid-state dye sensitized solar cells. *Alex. Eng. J.* (2016). <https://doi.org/10.1016/j.aej.2016.03.019>
27. M. Fathy, A. Gomaa, F. Taher, M. El-Fass, A.B. Kashyout, Optimizing the preparation parameters of GO and rGO for large scale production. *J. Mater. Sci.* (2016). <https://doi.org/10.1007/s10853-016-9869-8>
28. M.S. Abusaif, M. Fathy, M.A. Abu-Saied, A.A. Elhenawy, A.B. Kashyout, M.R. Selim, Y.A. Ammar, New carbazole-based organic dyes with different acceptors for dye-sensitized solar cells: synthesis, characterization, DSSC fabrications and density functional theory studies. *J. Mol. Struct.* (2021). <https://doi.org/10.21608/ejchem.2022.115059.5221>
29. A.E.H.B. Kashyout, S. El-Hashash, J. El Nady, M. Fathy, K. Shoueir, A. Wageh, R.A. Rassoul, Enhancement of the silicon solar cell efficiency by spin-coated polythiophene films embedded with gold or palladium nanoparticles on the rear contact. *ACS Omega* (2021). <https://doi.org/10.1021/acsomega.1c00761>

30. J.I. Langford, A.J.C. Wilson, Scherrer after sixty years: a survey and some new results in the determination of crystallite size. *J. Appl. Crystallogr.* (1978). <https://doi.org/10.1107/S0021889878012844>
31. V. Uvarov, I. Popov, Metrological characterization of X-ray diffraction methods for determination of crystallite size in nano-scale materials. *Mater. Charact.* (2013). <https://doi.org/10.1016/j.matchar.2006.09.002>
32. S.M. Algabry, K.R. Shoueir, A.E.H.B. Kashyout, M. El-Kemary, Engineering electrospun of in situ plasmonic AgNPs onto PANI@ PVDF nanofibrous scaffold as back surface support for enhancing silicon solar cells efficiency with the electrical model assessment. *Sustain. Mater. Technol.* (2022). <https://doi.org/10.1016/j.susmat.2021.e00380>
33. W. Yang, Y. Yang, A.L. Kaledin, S. He, T. Jin, J.R. McBride, T. Lian, Surface passivation extends single and biexciton lifetimes of InP quantum dots. *Chem. Sci.* (2020). <https://doi.org/10.1039/D0SC01039A>
34. T. Aihara, T. Tayagaki, Y. Nagato, Y. Okano, T. Sugaya, InGaP-based InP quantum dot solar cells with extended optical absorption range. *Jpn. J. Appl. Phys.* (2017). <https://doi.org/10.1021/acsam.8b01453>
35. S. Carenco, M. Demange, J. Shi, C. Boissière, C. Sanchez, P. Le Floch, N. Mézailles, White phosphorus and metal nanoparticles: a versatile route to metal phosphide nanoparticles. *Chem. Commun.* (2010). <https://doi.org/10.1039/D1NR02334A>
36. S. Yang, P. Zhao, X. Zhao, L. Qu, X. Lai, InP and Sn:InP based quantum dot sensitized solar cells. *J. Mater. Chem. A* (2015). <https://doi.org/10.1039/c5ta04925c>

Publisher's Note Springer Nature remains neutral with regard to jurisdictional claims in published maps and institutional affiliations.